JVST A
Journal of Vacuum Science & Technology A

Controlling conduction band alignment and carrier concentration in gallium-doped magnesium zinc oxide by reactive cosputtering

Cite as: J. Vac. Sci. Technol. A **39**, 022802 (2021); https://doi.org/10.1116/6.0000784
Submitted: 15 November 2020 . Accepted: 22 January 2021 . Published Online: 12 February 2021

Gavin Yeung, and Colin A. Wolden

JVST A
Journal of Vacuum Science & Technology A

ARTICLE

avs.scitation.org/journal/jva

Controlling conduction band alignment and carrier concentration in gallium-doped magnesium zinc oxide by reactive cosputtering

Cite as: J. Vac. Sci. Technol. A 39, 022802 (2021); doi: 10.1116/6.0000784
Submitted: 15 November 2020 · Accepted: 22 January 2021 ·
Published Online: 12 February 2021

Gavin Yeung and Colin A. Wolden

AFFILIATIONS

Department of Chemical and Biological Engineering, Colorado School of Mines, Golden, Colorado 80401

ABSTRACT

Gallium-doped magnesium zinc oxide (GMZO) holds promise as a UV transparent conducting oxide with tunable bandgap and conductivity, though there has been relatively limited exploration of the broad compositional space available. Conductive GMZO films were deposited by reactive cosputtering at room temperature followed by annealing. The contributions of alloying and the Burstein–Moss effect to the optical bandgap were decoupled through comparisons of as-deposited and annealed films. Compositional analysis in conjunction with electrical characterization was used to quantify the activation of Ga doping in MZO. Combinatorial synthesis was used to explore the optoelectronic performance over a broad composition space. Reactive cosputtering can be used to tailor GMZO properties for optoelectronic applications over a wide range of bandgaps (3.3–4 eV) and resistivity (10^{-3}–>100 Ω cm) through appropriate control of the Mg/Zn ratio and Ga content, respectively.

I. INTRODUCTION

Transparent conductive oxides (TCOs) play important roles in a host of optoelectronic devices including solar cells, flat panel displays, thin film transistors, and light emitting diodes.[1,2] Zinc oxide (ZnO) is a wide bandgap (~3.3 eV) semiconductor that is nontoxic, inexpensive, and widely employed as a TCO when doped with group III elements such as Ga or Al.[3–6] Furthermore, its bandgap may be further increased by alloying with Mg (MZO, $Mg_xZn_{1-x}O$). MZO alloys retain the wurtzite crystal structure, and the bandgap increases approximately linearly with Mg content up to $x \sim 0.4$ where the bandgap is ~4 eV.[7] As Mg is added, the valence band position remains essentially constant, but its electron affinity is reduced.[8] This aspect of MZO has been exploited in applications as the window layer in thin film solar cells, where the composition may be adjusted to optimize the conduction band offset with the absorber, including both copper indium gallium diselenide and cadmium telluride (CdTe) based devices.[9,10] These attributes have helped establish MZO as a leading emitter in CdTe-based solar cells.[11–13] One drawback of MZO is that it is highly resistive, and increasing the carrier concentration is a key to further enhancing device efficiency, particularly when coupled with absorbers that employ group V doping.[14,15]

Among group III dopants, gallium is preferred over aluminum due to its size, which is closer to zinc and results in less lattice distortion and thus improved mobility.[16] To date, most of the work on gallium-doped magnesium zinc oxide (GMZO) has focused on minimizing its resistivity for use as a UV transparent electrical contact.[16–19] The composition space explored to date is relatively limited as these studies are typically done using ceramic targets of fixed composition. Typical targets employ 2–3 wt. % Ga_2O_3 and low Mg content (<5%), and films are typically sputtered in an Ar ambient and yield resistivity values of ~10^{-3} Ω cm. Maejima *et al.*[20] deposited GMZO by cosputtering GZO and MgO targets, achieving resistivity as low as 6×10^{-4} Ω cm that increased with Mg content due to declines in both carrier concentration and mobility. Using reactive sputtering of metal alloy targets, Ma *et al.*[21] reported the most conductive GMZO films reported to date, with resistivity as low as 3×10^{-4} Ω cm and similar trends with respect to Mg content. Combinatorial synthesis of GMZO was explored using ZnO, Mg, and Ga_2O_3 targets in the presence of temperature gradients.[22] All films had similar resistivity values (~10^{-3} Ω cm), and there was surprisingly little variation with either Mg (4%–17%) or Ga (0.5%–3%) content.

Previous studies have all focused on conductive, degenerately doped films.[16–22] While ideal for forming electrodes that are both UV transparent and IR reflective, for application as an emitter layer in CdTe solar cells, it is desirable to have semiconducting GMZO

with carrier concentrations in the range of 10^{16}–10^{18} cm^{-3}.[14] Moreover, the ideal Mg:Zn ratio remains unknown for this application, and it is likely a function of the specific device architecture and processing conditions employed. This will continue to evolve with the recent shift to selenium alloying (CST: $CdSe_yTe_{1-y}$) and group V doping, where the Se content at the interface may vary significantly ($y = 0.05$–0.15).[15,23–25] In addition, most MZO films appear to be unstable when processed at elevated temperatures in the presence of oxygen.[23,26,27] This is attributed to the loss of oxygen vacancies or zinc interstitials introduced by sputtering in an Ar environment, creating an S kink in the J-V curves of resulting devices. Previously, we employed combinatorial reactive sputtering to optimize stable MZO emitters for CdTe solar cells produced across multiple laboratories.[8] Moreover, these films were robust to subsequent $CdCl_2$ activation steps employing oxygen, with resulting devices displaying good rectification. In this work, we extend this approach to fabricate GMZO films with controlled bandgap and carrier concentration using Zn, Mg, and Ga_2O_3 targets. Synthesis of combinatorial libraries was used to efficiently explore the large composition space and demonstrate the range of properties that may be obtained through this approach.

II. EXPERIMENT

MZO and GMZO films were deposited by reactive cosputtering in an AJA Orion-5 sputtering system. Glass slides and silicon wafer substrates were used to determine the properties of the deposited films, including bandgap, resistivity, and thickness. GMZO films are deposited at ambient temperature by cosputtering Zn (Kurt J. Lesker: 99.99%), Mg (Kurt J. Lesker: 99.95%), and Ga_2O_3 (Plasmaterials: 99.99%) using 2 in. diameter targets. Figure 1 displays a photograph showing the positions of Zn, Mg, and Ga_2O_3 targets with the substrate for combinatorial sputtering. The center of the Mg and Zn targets 16 cm apart, and the Ga_2O_3 target is offset 5 cm perpendicular from the midpoint of the Zn-Mg axis. The substrate is placed 10 cm above the target plane in this sputter up arrangement.

Sputtering was performed with no intentional heating in an argon/oxygen ambient supplied in a 13:2 ratio at P = 5.5 mTorr. The Zn target employed DC sputtering with the current fixed at 45 mA for all films deposited in this work. The RF power supplied to the Mg and Ga_2O_3 targets was varied from 100 to 150 and 10 to 110 W, respectively. Uniform films were produced with substrate rotation, while combinatorial libraries were formed with the substrate fixed as shown in Fig. 1. After deposition, films were annealed in air or 10^{-6} Torr vacuum at temperature ranges from 200 to 500 °C for 2 h and then allowed to cool naturally under vacuum to ambient temperature over several hours.

Films were examined in their as-deposited state and after annealing in both air and vacuum. A J. A. Woollam M-2000 ellipsometer was used to determine the thickness of the deposited film on silicon witness samples. An Agilent Cary 5000 UV-vis is used to determine the UV-vis spectra, and Tauc plots are used to extract the bandgap. An Ossila four-point probe is used to determine the sheet resistance of the deposited film on glass slides. A Bio-Rad HL5500PC Hall effect measurement system is used to measure the carrier concentration and mobility of the deposited film on glass slides. Inductively coupled plasma atomic emission spectroscopy is employed to determine the elemental content of deposited films by dissolving the film in aqua regia. To facilitate comparison between MZO and GMZO films, the Mg/Zn ratio and level of Ga doping are reported in this work using the molar ratios x = Mg/(Mg + Zn) and y = Ga/(Ga + Zn + Mg), respectively.

III. RESULTS AND DISCUSSION

A. Effect of annealing conditions

Figure 2 shows the resistivity of uniform sputtered 3% $Ga/Mg_{0.05}Zn_{0.95}O$ films as a function of annealing temperature and ambient. As-deposited films at this condition had a resistivity of ~10 Ω cm, indicating that Ga was not significantly activated. Annealing in air up to 300 °C reduces the resistivity to ~1 Ω cm,

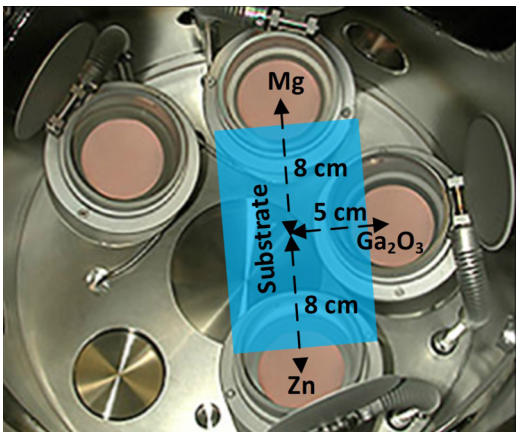

FIG. 1. Top view photograph of the sputtering geometry employed. Reprinted with permission from AJA International, Inc. (Ref. 28).

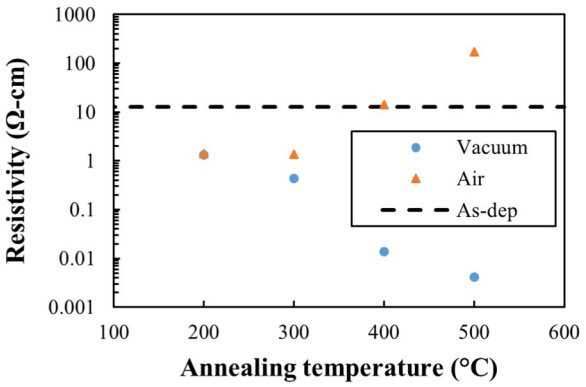

FIG. 2. Resistivity of uniform 3% $Ga/Mg_{0.05}Z_{0.95}O$ film as a function of annealing temperature in air and vacuum.

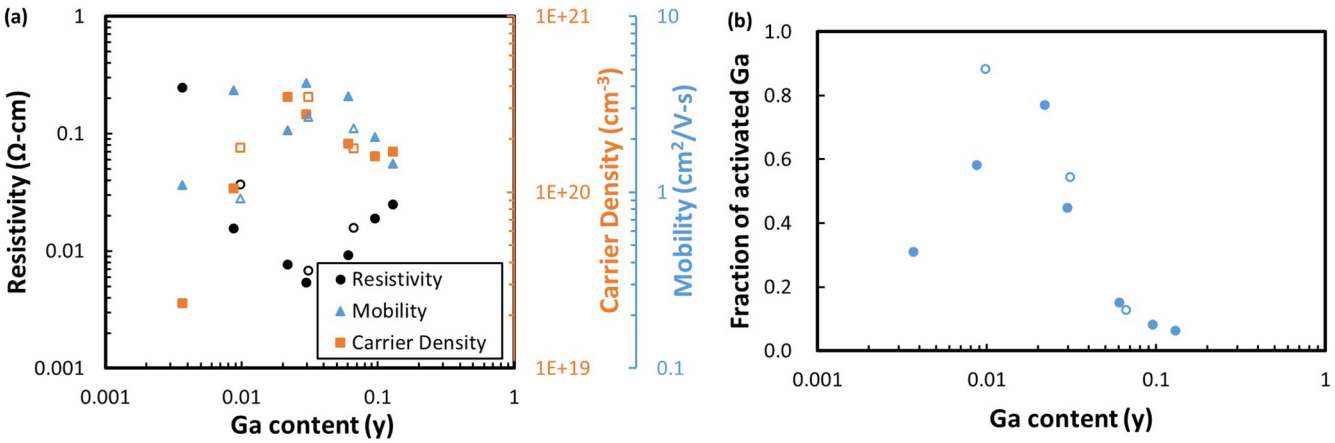

FIG. 3. (a) Resistivity, carrier concentration, and mobility and (b) Ga activation of annealed $Mg_xZn_{1-x}O$ films as a function of Ga content for x = 0.05 (solid symbols) and x = 0.10 (open symbols).

which may be caused by slightly activating Ga and increasing the carrier concentration. Further increasing the annealing temperature increased the resistivity. There is likely a competition between activating Ga through its substitution for Zn/Mg in the lattice and its oxidation to an inactive form. By annealing in vacuum, this second pathway is eliminated and the resistivity improves exponentially with temperature to a minimum value of 4×10^{-3} Ω cm at T = 500 °C. It is also likely that vacuum annealing introduces point defects such as oxygen vacancies that contribute to the increase carrier concentration as has been observed with intrinsic MZO films.[29] Higher temperatures could possibly further increase the conductivity, but such experiments were limited by the stability of the soda lime glass substrates. All annealed samples discussed through the remainder of this paper received vacuum annealing at T = 500 °C.

B. Optimal gallium doping

Figure 3(a) displays the electrical properties of annealed GMZO films as a function of Ga content, with fixed Mg content at x = 0.05 or 0.10. In both cases, a clear minimum in resistivity was achieved at a Ga content of y ~ 0.03. To first order, the resistivity scaled with the inverse of carrier concentration, which were order of 10^{20} cm^{-3}. There was not a strong trend in mobility, with values of 2 ± 1 cm^2/V s, though the highest value was achieved at the optimal power level and beyond that the mobility slowly declined as one would expect due to the increase in scattering centers. The resistivity values in the higher Mg content films were about twice the x = 0.05 series, and this was attributed primarily to decreased mobility, as the carrier concentration was nominally unchanged. The efficacy of Ga doping is displayed in Fig. 3(b). Donor

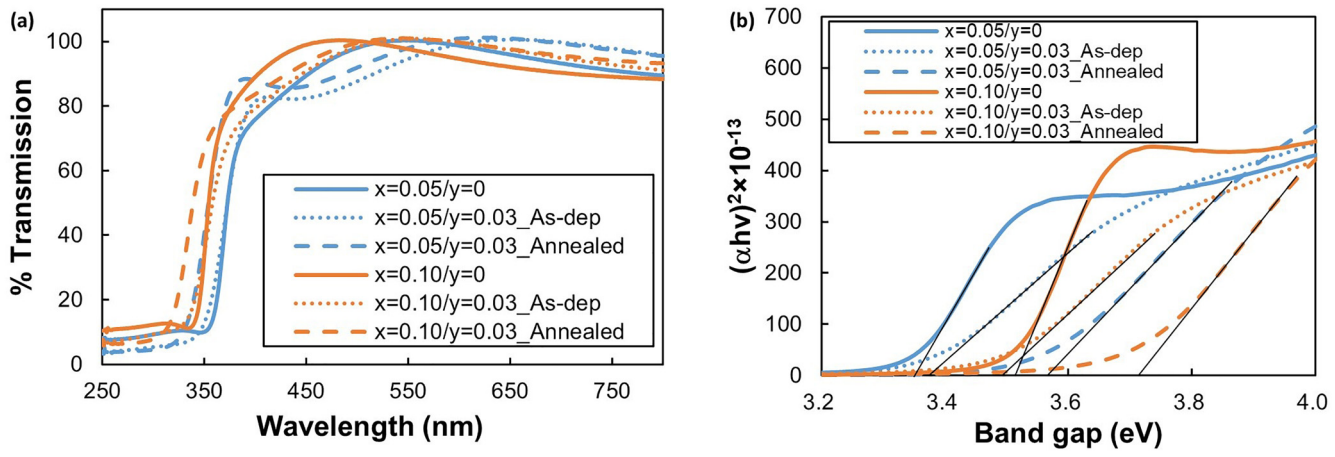

FIG. 4. (a) Optical transmission and corresponding (b) Tauc plots of MZO and GMZO samples with different Mg content before and after vacuum annealing.

ionization is most efficient at gallium levels of 0.9%–2%. At higher concentrations, the degree of activation falls sharply as the carrier concentration declines despite the increased amount of Ga.

C. Bandgap dependence on alloying and doping

In conductive GMZO films, the bandgap extracted from optical transmission measurements reflects both the intrinsic MZO bandgap as well as the contributions due to the Burstein–Moss shift.[18,19,22] The Burstein–Moss effect[30,31] occurs in degenerately doped semiconductors, $N_D > 6 \times 10^{18}$ cm^{-3} for ZnO,[32] where excess carriers fill all of the allowed states within the bandgap and push the Fermi level position above the conduction band. Decoupling these two components was done by comparing the optical transmission of as-deposited and annealed films as illustrated in Fig. 4. The transmission spectra of as-deposited GMZO films are nominally identical to their insulating MZO counterparts deposited at the same conditions [Fig. 4(a)]. Bandgaps extracted from Tauc plots are nominally identical, and these values are representative of the intrinsic bandgap [Fig. 4(b)] since the Burstein–Moss effect is negligible. The absorption edge of intrinsic MZO films is sharper than that of as-deposited GMZO [Fig. 4(b)], suggesting that Ga addition introduces defect states around the band edge but no appreciable change in its value. After annealing the GMZO spectra shift to shorter wavelengths (dashed lines), instigating a blue shift (~0.2 eV) that is attributed to the Burstein–Moss effect. The absorption edge also becomes slightly sharper, suggesting the removal of some defect states during annealing.

D. Combinatorial GMZO libraries

To more efficiently explore the broad GMZO compositional phase, space combinatorial libraries were fabricated by not rotating the substrate during deposition. Figure 5 displays the optical properties of libraries fabricated with the Zn and Mg parameters fixed and varying the power applied to the Ga_2O_3 target. The data presented are obtained from the centerline between the Zn and Mg targets, with x = 0 being equidistant from the two targets. The optical bandgap of the as-deposited films was independent of the level of gallium doping, and these values are indicated by the gray curve, with the observed variability among samples represented by its width. As discussed above the as-deposited bandgap is representative of the MZO composition, and the Mg content was estimated using the relationship between optical bandgap and composition for $Mg_xZn_{1-x}O$ established by Minemoto *et al.*[7] and confirmed by our own ICP results. For these deposition conditions, the Mg content increases parabolically across the library from x ~ 0.02 on the Zn rich side of the library to x ~ 0.25 on the Mg rich side.

At the lowest Ga doping level (y ~ 0.003), the bandgap of the annealed library was nominally identical to the as-deposited state. Thus, while the film conductivity increased upon annealing the level of doping was not degenerate. For all the other Ga levels, the optical bandgap increased after annealing, and the degree of departure from the as-deposited curve is the contribution of the Burstein–Moss shift that reflects the carrier concentration (N_D)

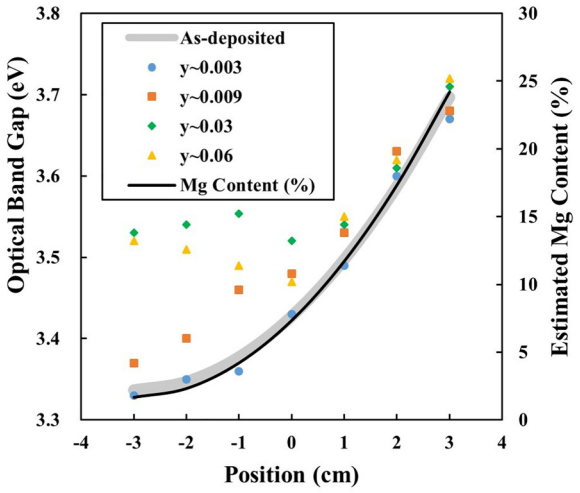

FIG. 5. Variation of the optical bandgap of GMZO along the centerline between the Zn and Mg targets before (gray band) and after (points) annealing from combinatorial libraries formed with the Zn and Mg targets fixed and varying the Ga_2O_3 power. Mg content was estimated based on the bandgap of the as-deposited films and the Ga content (y) at the center of each library is indicated in the legend.

through the following relationship:

$$\Delta E^{BM} = \frac{h^2}{8\pi^2 m^*}(3\pi^2 N_D)^{2/3}, \quad (1)$$

where h is Planck's constant and m^* is the effective mass. The optical shifts are consistent with the electrical measurements (Fig. 3). At the optimal doping level (y ~ 0.03), the optical bandgap is nominally independent of Mg content for much of the range examined (x < 0.15), consistent with other reports of high conductivity GMZO.[20,21] Comparison of as-deposited and annealed bandgaps allows the contributions of intrinsic bandgap and Burstein–Moss effect to be effectively decoupled.

Figure 5 shows that the efficacy of gallium doping diminishes as the Mg content increases, consistent with the literature.[20,21] For Mg content x > 0.15, the optical bandgap after annealing is similar to as-deposited films at all Ga levels. There are a number of possible reasons for this, including an increase in donor ionization energy and formation of compensating acceptor states.[4,33] The amphoteric nature of Mg has been previously documented in metal oxide TCOs.[34] There is also an increase in effective mass as Mg is added,[33] which is consistent with the decrease mobility observed in uniform films deposited with higher Mg content (Fig. 3).

For application as a window layer in CdTe-based solar cells, the key parameters for MZO are its carrier concentration (N_D) and conduction band offset (ΔE_C) with the absorber.[14] Figure 6 displays the combination of values that may be obtained over 3 in. square combinatorial libraries fabricated in our laboratory. Figure 6 plots the electrical resistivity versus the intrinsic bandgap, which is based on the as-deposited transmission. As before, the points on the

graph are obtained along the centerline between the Zn and Mg targets. The shaded regions around the points approximate of the range of bandgaps and resistivity that are observed across these libraries. Within a library, there are minor variations in optical bandgap (±0.05 eV) and more significant variations in resistivity (± up to an order of magnitude) in the transverse direction. The latter reflects the Ga profile which is orthogonal to the Zn-Mg axis (Fig. 1). The estimate of the conduction band alignment was based on assuming a $\Delta E_C = -0.2$ eV for a ZnO:CdTe heterojunction,[35] and that increases in bandgap only reflect shifts in the MZO conduction band position. This is of course an oversimplification and the true values could be slightly shifted in either direction and part of the change in bandgap is due to shifts in the valence band position.[33] Thus, for a library with bandgap variation of 0.5 eV, the variation in ΔE_C would be ~0.4 eV. Nevertheless, the axes are representative of the range of values that may be obtained through this approach.

Device simulations suggest optimal values of $N_D \sim 10^{17}$–10^{18} cm^{-3} and $\Delta E_C \sim +0.2$ eV, respectively,[14] and this combination of values is achievable within the parameter space available. The power supplied to the Zn and Mg targets controls the range of bandgap (ΔE_C) that may be obtained. There is an exponential relationship between resistivity and bandgap, as evidenced by the linear shape of the combinatorial libraries on the semilog plot in Fig. 6. The slope reflects the degree that Mg addition impacts Ga activation. Extracting the carrier concentration requires knowledge of the mobility. As with the uniform samples [Fig. 3(a)], it was observed that the mobility was largely independent of the Ga doping level when they are degenerately doped, but it was a strong function of the Mg/Zn ratio. The average mobility of degenerately doped GMZO ($N_D \geq 10^{19}$ cm^{-3}) from multiple libraries is plotted on the secondary axis of Fig. 6. The value declines exponentially from 7.2 $cm^2/V\,s$ at 3.35 eV (x ~ 0.02) to 0.17 $cm^2/V\,s$ at 3.85 eV (x ~ 0.35). In these degenerately doped libraries, the change in carrier concentration is relatively modest, declining from $>10^{20}$ in Zn-rich films to ~10^{19} cm^{-3} as Mg is added. For semiconducting GMZO (i.e., y ~ 0.003), the variation in mobility with Mg content was modest (1–5 $cm^2/V\,s$), and as such carrier concentration ranged from 10^{19} cm^{-3} at the high end to 10^{17} cm^{-3} and likely lower, but values below this threshold could not be reliably measured. Thus, this approach appears suitable for engineering both the conduction band alignment and emitter doping level independently through appropriate control of the Zn/Mg and Ga_2O_3 sputtering conditions, respectively.

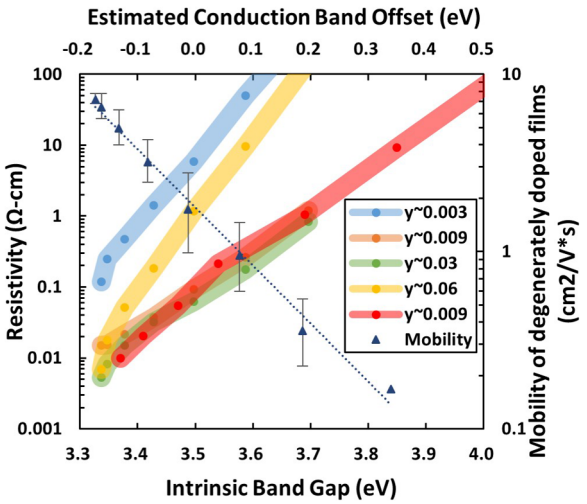

FIG. 6. Map showing the combinations of electrical resistivity, mobility, and intrinsic bandgap that were achieved for selected libraries, where y indicates the nominal Ga content at its center. The circles are bandgap/resistivity data recorded along the centerline between the Zn and Mg targets, and the shaded regions illustrate the range observed across 3 × 3″ library. The triangles are the average mobility from these libraries at selected bandgaps which can be used to infer carrier concentration (N_D). The estimated band offset assumes $\Delta E_C = -0.2$ eV for a ZnO:CdTe heterojunction, and that increases in the bandgap only shift the MZO conduction band position.

IV. CONCLUSIONS

Reactive cosputtering was shown to be capable of producing both semiconducting and degenerately doped GMZO. The MZO composition may be reliably estimated from the optical bandgap of as-deposited films, as vacuum annealing was required to activate Ga with optimal doping efficiency achieved at 1%–2% Ga. GMZO properties for optoelectronic applications may be tuned over a broad range of bandgaps (3.3–4 eV) and resistivity (10^{-3}–>100 Ω cm) through appropriate control of the Mg/Zn ratio and Ga content, respectively. In degenerately doped GMZO ($N_D > 10^{19}$ cm^{-3}), the electrical mobility declined exponentially with Mg content. In contrast, the mobility was relatively constant in semiconducting GMZO and the carrier concentration varied orders of magnitude. The ability to independently control these properties in the cosputtering environment is expected to be useful for optimizing the performance of optoelectronic devices including CdTe based solar cells.

ACKNOWLEDGMENTS

We are grateful to the National Science Foundation (NSF) through Award No. CBET-1706149. We would like to thank Zhenyu Zhang and Saeed A. Vaselabadi for assistance with annealing experiments.

REFERENCES

[1]T. Minami, J. Vac. Sci. Technol. A **17**, 1765 (1999).
[2]E. Fortunato, D. Ginley, H. Hosono, and D. C. Paine, MRS Bull. **32**, 242 (2007).
[3]D. C. Look, D. C. Reynolds, J. R. Sizelove, R. L. Jones, C. W. Litton, G. Cantwell, and W. C. Harsch, Solid State Commun. **105**, 399 (1998).

[4]K. Ellmer and A. Bikowski, J. Phys. D **49**, 413002 (2016).
[5]J. N. Duenow, T. A. Gessert, D. M. Wood, A. C. Dillon, and T. J. Coutts, J. Vac. Sci. Technol. A **26**, 692 (2008).
[6]E. Fortunato *et al.*, Sol. Energy Mater. Sol. Cells **92**, 1605 (2008).
[7]T. Minemoto, T. Negami, S. Nishiwaki, H. Takakura, and Y. Hamakawa, Thin Solid Films **372**, 173 (2000).
[8]Y. Samoilenko *et al.*, Sol. Energy Mater. Sol. Cells **210**, 110521 (2020).
[9]K. Tanaka, T. Minemoto, and H. Takakura, Solar Energy **83**, 477 (2009).
[10]J. M. Kephart, J. W. McCamy, Z. Ma, A. Ganjoo, F. M. Alamgir, and W. S. Sampath, Sol. Energy Mater. Sol. Cells **157**, 266 (2016).
[11]A. H. Munshi, J. Kephart, A. Abbas, J. Raguse, J. N. Beaudry, K. Barth, J. Sites, J. Walls, and W. Sampath, IEEE J. Photovoltaics **8**, 310 (2018).
[12]A. H. Munshi, J. M. Kephart, A. Abbas, T. M. Shimpi, K. L. Barth, J. M. Walls, and W. S. Sampath, Sol. Energy Mater. Sol. Cells **176**, 9 (2018).
[13]T. Ablekim *et al.*, ACS Energy Lett. **5**, 892 (2020).
[14]T. Ablekim, E. Colegrove, and W. K. Metzger, ACS Appl. Energy Mater. **1**, 5135 (2018).
[15]W. K. Metzger *et al.*, Nat. Energy **4**, 837 (2019).
[16]H.-C. Lu, J.-C. Jou, and C.-L. Chu, Surf. Coat. Technol. **231**, 539 (2013).
[17]H. Kang, Z. Lu, Z. Zhong, and T. Zhang, J. Mater. Sci. **29**, 2874 (2017).
[18]W. Wei, C. Jin, J. Narayan, and R. J. Narayan, Solid State Commun. **149**, 1670 (2009).
[19]J. M. Kephart and W. S. Sampath, "Gallium-doped magnesium zinc oxide (GMZO) transparent conducting oxide layers for CdTe thin-film photovoltaics," in *2015 IEEE 42nd Photovoltaic Specialist Conference (PVSC)*, New Orleans, LA, 14-19 June 2015, (IEEE, New York, 2015), pp. 1–4.
[20]K. Maejima, H. Shibata, H. Tampo, K. Matsubara, and S. Niki, Thin Solid Films **518**, 2949 (2010).
[21]Q.-B. Ma, H.-P. He, Z.-Z. Ye, L.-P. Zhu, J.-Y. Huang, Y.-Z. Zhang, and B.-H. Zhao, J. Solid State Chem. **181**, 525 (2008).
[22]P. P. Rajbhandari, A. Bikowski, J. D. Perkins, T. P. Dhakal, and A. Zakutayev, Sol. Energy Mater. Sol. Cells **159**, 219 (2017).
[23]T. Ablekim *et al.*, IEEE J. Photovoltaics **9**, 888 (2019).
[24]X. Zheng *et al.*, APL Mater. **7**, 071112 (2019).
[25]T. A. M. Fiducia *et al.*, Nat. Energy **4**, 504 (2019).
[26]D.-B. Li, Z. Song, S. S. Bista, R. A. Awni, C. R. Grice, L. Chen, and Y. Yan, "Get rid of S-kink in MZO/CdTe solar cells by performing CdCl2 annealing without oxygen," in *2019 IEEE 46th Photovoltaic Specialists Conference (PVSC)*, Chicago, IL, 15–21 June 2019, (IEEE, New York, 2019), pp. 3015–3017.
[27]F. Bittau, S. Jagdale, C. Potamialis, J. W. Bowers, J. M. Walls, A. H. Munshi, K. L. Barth, and W. S. Sampath, Thin Solid Films **691**, 137556 (2019).
[28]See http://www.ajaint.com/atc-orion-series-sputtering-systems.html for AJA International Inc. (July 1). *ATC Orion Series Sputtering Systems*.
[29]W. W. Liu, B. Yao, Y. F. Li, B. H. Li, Z. Z. Zhang, C. X. Shan, J. Y. Zhang, D. Z. Shen, and X. W. Fan, J. Mater. Sci. **45**, 6206 (2010).
[30]E. Burstein, Phys. Rev. **93**, 632 (1954).
[31]T. S. Moss, Proc. Phys. Soc. London Ser. B **67**, 775 (1954).
[32]A. P. Roth, J. B. Webb, and D. F. Williams, Solid State Commun. **39**, 1269 (1981).
[33]Y. Ke, S. Lany, J. J. Berry, J. D. Perkins, P. A. Parilla, A. Zakutayev, T. Ohno, R. O'Hayre, and D. S. Ginley, Adv. Funct. Mater. **24**, 2875 (2014).
[34]O. Bierwagen, Semicond. Sci. Technol. **30**, 024001 (2015).
[35]H. Fardi and F. Buny, Int. J. Photoenergy **2013**, 576952 (2013).
[36]B. Good, T. Ablekim, I. S. Khan, M. O. Reese, A. Zakutayev, and W. K. Metzger, J. Phys. D **54**, 034002 (2020).